Korean J. Chem. Eng., 34(10), 2570-2583 (2017)
DOI: 10.1007/s11814-017-0180-4

pISSN: 0256-1115
eISSN: 1975-7220

Energy management in multi stage evaporator through a steady and dynamic state analysis

Om Prakash Verma, Gaurav Manik†, and Toufiq Haji Mohammed

Department of Polymer and Process Engineering, Indian Institute of Technology Roorkee, India
(*Received 15 December 2016 • accepted 2 July 2017*)

Abstract−Increasing energy demand, high cost of energy and global warming issues across the globe require energy-intensive industries, such as paper mills to improve energy efficiency. Multi-stage evaporators used to concentrate the black liquor in such mills form its most energy consuming unit and require a strong understanding of steady and unsteady state behavior to ensure energy savings. The modeling of nonlinear heptads' effect system yielded a set of complex nonlinear algebraic and differential equations that are analyzed using Interior-point method and state space representation. Dynamic response of product concentration and system vapor temperatures along with system stability and controllability have been explored by disturbing the flow rate, concentration and temperature of feed, and fresh steam flow rate. Simulations predict that steam flow rate, feed flow rate and its concentration invariably are major controlling factors (in decreasing order) of vapor temperature and product concentration. The interactive behavior between different effects translates into slower responses of the effects with increasing separation from disturbance source. This steady state and transient study opens many new explanations to this relatively less explored area and helps to propose and implement industrial PID controllers to reduce steam consumption and control product quality.

Keywords: Energy Efficiency, Evaporative Heat Transfer, Multi-stage Evaporator, Nonlinear Dynamic Model, PID Controller, State Space Representation

INTRODUCTION

The pulp and paper industry is one of the world's fastest growing and highest priority industries due to its energy intensive nature. For instance, the Indian pulp and paper industry which ranks fifteenth globally in terms of size [1] ranks sixth among the most energy intensive industries of India and fourth globally with an energy requirement of about 10 Mtpa of coal and 10.6 GWh of electricity. A ~11-15 ton consumption of steam and ~1,500-1,700 kWh of electricity per ton paper accrues to a huge annual specific energy requirement of ~52 GJ per ton paper. The consumption of fuel, primarily coal, utilized in producing steam for various plant heating processes, forms ~15-20% of total production cost in such industries. This is significantly high compared to non-Indian pulp and paper mills [2,3]. However, a major share of this steam is used within the pulping process (digester, evaporator and washing), of which the Kraft evaporative recovery process is the most energy taxing and consumes more than 24-30% of fresh steam out of total plant consumption [4,5].

The spent liquor and its dissolved contaminants, collectively referred to as weak *black liquor*, derived from the Kraft process, is sent to the chemical recovery process to regenerate digestion chemicals via a *white liquor* recycle [6-8]. While this takes care of the chemical recovery, the evaporative process employing a multiple stage evaporator (MSE) unit helps to improve the energy recovery in boiler [9]. In the MSE, the waste weak black liquor undergoes concentration from an initial concentration of ~12-14% to ~40-55% solids, which is used as fuel in boiler. The concentrated black liquor has been described globally as potentially the fifth most important fuel.

The increasing costs of fuel/energy as well as stringent pollution regulations to control greenhouse gaseous emissions and water pollution have subjected Indian pulp and paper mills to tremendous pressures. Keeping this in mind, many researchers in the last decade have developed and proposed different energy reduction schemes (ERS) to maximize steam economy (SE) and minimize steam consumption (SC) based on feeding mode of weak liquor and fresh live steam [10]. To achieve this energy efficiency, the MSE system selected for the investigation is a Heptads' effect evaporator (HEE) operated with backward feed flow (BFF). Such an operation, predominantly used in many Indian pulp and paper mills, involves live fresh steam and weak black liquor moving counter-currently through various effects.

A large number of mathematical models for the MSE system for different process industries including pulp and paper mill have been proposed, but most of the models have been reported majorly for the steady state process condition [4,11-21]. These steady state models have been specifically designed and analyzed to improve the energy efficiency parameters namely SE and SC. The reported steady state models may be differentiated on the basis of their inherent linearity and nonlinearity properties. A set of linear algebraic equations have been developed, after making appropriate assumptions, to simplify solution for different ERS [20,22-24]. This, however, may take the system away from reality. Nonlinear models have also been developed, linearized analytically [25] and solved using numerical

†To whom correspondence should be addressed.
E-mail: manikfpt@iitr.ac.in

iterative approaches such as Gauss elimination method [26]. However, such iterative methods are found to yield non-feasible results with the variation of operating conditions. To eliminate such issues, few of the models have been developed based on the concepts of cascade algorithm [14,27] and pinch analysis [28,29].

The steady state analysis has thus been well explored in the previously published literature, but the dynamic analysis of MSE has neither been extensively investigated nor well documented. Further, the available literature based on the dynamic study has been limited only to single, double and triple effects [30,31]. The understanding of system dynamic behavior carries immense significance as this may help effective system control to eliminate undesirable transient disturbances from desired steady state conditions which culminates in an efficient energy management of process [32].

The standard state space model was first presented and applied to linearize the nonlinear dynamics of a double effect evaporator [33]. In this sequence, a nonlinear regulator has been designed based on Riemannian geometric approach to solve the nonlinear dynamics but was limited to a single- and double-effect evaporator [34,35]. Similar models have been proposed for double-effect evaporator to identify steam and concentration disturbances in process and dynamics response used to control them [36]. Later, the dynamic response was formulated for the different ERS for a higher number of effects in evaporator system (up to i=7) [10,37]. The dynamic response has been evaluated to study the open loop and closed loop response, and to further design the PID controller for controlling the concentration of the tomato paste product of a double-effect evaporator [38].

Besides modeling the response based on first principles approach, some studies present artificial intelligence techniques such as Auto-Regressive model, Artificial Neural Network and Fuzzy Logic Controller to empirically develop the dynamics and then to design the controller [39,40]. The combination of phenomenological and neural networks approach over first principle approach demonstrates reduced complexities involved in modeling and simulation of system. The approach has been implemented to study the dynamic response of even higher number of effects (10) [41].

On the basis of the mentioned studies, this work attempts to analytically linearize a nonlinear model of HEE using the state space representation. The state space representation, in contrast to other solution techniques, helps to evaluate system stability and controllability through eigenvalue stability condition and Kalmans' controllability test with ease. The steady state information required for simulating the model was obtained by using an efficient I-PM algorithm that overrides the issues of divergence and initial guess requirement found with conventional algorithms. The algorithm's efficiency to explore parameter space has been compared with previously published bioinspired search techniques such as genetic algorithm (GA) [2].

This work investigates the transient response of product concentration and vapor temperature due to a ±10% disturbance in possible process disturbances: liquor feed-flow, concentration, temperature and fresh steam flow. This development is important as it explains the impact that process disturbances would have on the product parameters that dictate the product quality and cost. Further, this work expects to fill the gap in literature by identifying which of the process disturbances assume more weight in influencing the product parameters heavily and which do not. This topic has been relatively less explored in the past and has been extended to control product quality through an improved dynamic response via PID control implementation. The simulations for the work were performed on Intel(R) Xeon(R) CPU E5-1650 @3.20 GHz workstation using a developed code of MATLAB (R2013a version).

PROCESS DESCRIPTION

It has been reported that BFF provides a more suitable configuration than the forward-feed and mixed-feed configurations due to its relatively high SE and low steam consumption [20]. Here, the liquor is exposed to relatively higher temperatures, thereby increasing the heat transfer rate due to a greater reduction in viscosity. Considering these pertinent advantages of BFF configuration, it has been considered for the present investigation to study the dynamic response. There is also a need to have an improved understanding of the dynamics of such a system to design a better control strategy so that parameters set-point can be maintained or tracked and the disturbances rejected effectively. This will also help identify the dominating disturbance that could significantly impact product quality out of a given set of possible system disturbances.

The dynamic response requires identification of steady-state condition or parameters around which the transient model of system may be developed. Hence, prior to simulating system transience a steady-state analysis was performed using the operational data acquired from a paper mill located nearby Saharanpur, U.P., India

Table 1. Operating parameters of HEE (Data presented here has been taken from a nearby paper mill, Saharanpur, U.P., India)

Parameter	Abbreviation (unit)	Value (s)
Total number of effects	i	07
Inlet black liquor concentration	X_f	0.118
Inlet liquor temperature	T_f (in ^oC)	65
Feed flow rate of black liquor	L_f (in kg/sec)	15.611
7^{th} Effect vapor temperature	T_7 (in ^oC)	52
Heat transfer area	A_1-A_2, A_3-A_6 and A_7 (in m^2)	540, 660 and 690
Inlet liquor enthalpy	h_f (kJ/h)	254.81
Exit latent heat of vaporization	λ_8 (kJ/h)	2379
Mass hold-up for each effects	M_i (kg)	0.833

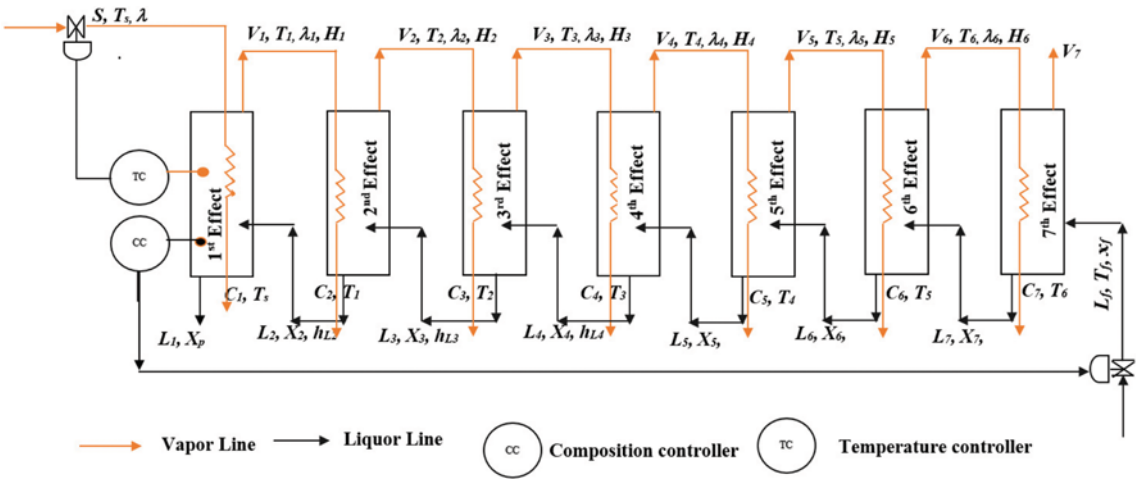

Fig. 1. Backward feed heptads' effect evaporator.

which is presented in Table 1.

The weak black liquor enters at the seventh effect (coldest) with flow rate, L_f, concentration, X_f, and temperature, T_f, and after evaporation of the liquor moves counter-currently to the steam in the successive effects. The concentrated black liquor as a product is obtained from the first effect (hottest) where the fresh steam with flow rate **S**, and temperature, T_s, is introduced. A block diagram representation of the HEE system is illustrated in Fig. 1, which indicates how the sub-systems relate to each other. The heptad's effects are numbered from left to right as first to seventh effects, respectively. V_i is the flow rate of vapor emanating from the overhead of i^{th} effect with temperature, T_i, respectively. The concentrated liquor products obtained from first to seventh effects are X_p, X_2, X_3… to X_7 with temperature, T_1, T_2…. to T_7 respectively.

MODEL DEVELOPMENT

1. Steady State Model

The steady state HEE model consists of a set of fourteen nonlinear algebraic equations obtained after applying the first principles laws and empirical correlations of thermo-physico parameters, enthalpy of black liquor, h_L, vapor, H, and condensate, h_c and latent heat of vaporization, λ. The assumptions made to formulate the model are listed below:

(i) The variation in composition, temperature and boiling point rise in each effects and heat loss to the surrounding is negligible.

(ii) The black liquor enthalpy is dependent on the temperature and concentration.

(iii) The black liquor and vapor produced at each effect are in thermal equilibrium.

Energy balance around the first effect involves the following–[Enthalpy of liquor entering from second effect with sensible heat] +[Latent heat of steam entering the vapor chest]=[Enthalpy of vapor leaving the effect]+[Enthalpy of liquor leaving the effect], which gives:

$$S\lambda_1+L_2h_2-L_1h_1-(L_2-L_1)H_2=0 \quad (1)$$

The heat transfer around shell-tube interface in first effect yields Eq. (2),

$$U_1A_1(T_1-T_2)=S\lambda_1 \quad (2)$$

Since, $V_i=L_i-L_{i-1}$, hence, for the remaining effects i=2-6, the Eqs. (1)-(2) may be generalized by Eqs. (3)-(4) as below-

$$(L_i-L_{i-1})\lambda_i+L_{i+1}h_{i+1}-L_ih_i-(L_{i+1}-L_i)H_{i+1}=0 \quad (3)$$

$$U_iA_i(T_i-T_{i+1})=(L_i-L_{i-1})\lambda_i \quad (4)$$

For the seventh effect the model equations are:

$$(L_7-L_6)\lambda_7+L_fh_f-L_7h_7-(L_f-L_7)H_8=0 \quad (5)$$

$$U_7A_7(T_7-T_8)=(L_7-L_6)\lambda_7 \quad (6)$$

The set of equations represented by Eqs. (1)-(6) for the seven effects translate into fourteen nonlinear algebraic equations that formulate the steady state model to be optimized and solved.

2. Dynamic Model

The present work extends the dynamic model development for HEE system based on the previous investigations [10,38,42,43] and the developed model is validated with earlier results [10] for a backward feed configuration liquor flow. The HEE model consists of a set of fourteen nonlinear first-order differential algebraic equations under similar conditions above.

2-1. Mass Balance

$$\text{At first to sixth effects: } \frac{dM_i}{dt}=L_{i+1}-L_i-V_i, \text{ Where i=1 to 6} \quad (7)$$

$$\text{Last effect: } \frac{dM_7}{dt}=L_f-L_7-V_7 \quad (8)$$

2-2. Total Mass Component Balance

$$\text{At first effect: } \frac{d(M_1X_p)}{dt}=L_2X_2-L_1X_p \quad (9)$$

$$\text{On simplification for the first effect: } \frac{dX_p}{dt}=\frac{L_2(X_2-X_p)+X_pV_1}{M_1} \quad (10)$$

Similarly, for the second to sixth effects:

$$\frac{dX_i}{dt}=\frac{L_{i+1}(X_{i+1}-X_i)+X_iV_i}{M_i}, \text{ Where i=1 to 6} \quad (11)$$

$$\text{Last effect: } \frac{dX_7}{dt} = \frac{L_f(X_f - X_7) + X_7 V_7}{M_7} \quad (12)$$

2-3. Total Energy Balance

At the first effect:

$$\frac{d[M_1 h(T_1, X_p)]}{dt} = L_2 h(T_2, X_2) + S\lambda_0 - L_1 h(T_1, X_p) - V_1 H(T_1) \quad (13)$$

On solving Eq. (13):

$$\frac{d[h(T_1, X_p)]}{dt} = \frac{L_2[h(T_2, X_2) - h(T_1, X_p)] + S\lambda(T_s) - V_1[H(T_1) - h(T_1, X_p)]}{M_1} \quad (14)$$

In similar way, for second to sixth effects:

$$\frac{d[h(T_i, X_i)]}{dt} = \frac{L_{i+1}[h(T_{i+1}, X_{i+1}) - h(T_i, X_i)] + V_i\lambda(T_i) - V_i[H(T_i) - h(T_i, X_i)]}{M_i}, \quad (15)$$

Where i=2 to 6

Last effect:

$$\frac{d[h(T_7, X_7)]}{dt} = \frac{L_f[h(T_f, X_f) - h(T_7, X_7)] + V_6\lambda(T_6) - V_7[H(T_7) - h(T_7, X_7)]}{M_7} \quad (16)$$

The empirical correlations developed earlier [2,14,20,44] for the enthalpy of black liquor (h_L), latent heat of vaporization (λ), enthalpy of vapor (**H**) and enthalpy of condensate (h_c) are presented in Eqs. (17)-(20).

$$H_i(T) = -0.0002045T_i^2 - 1.677T_i + 2507 \quad (17)$$

$$h_{c_i} = 4.15T_i \quad (18)$$

$$\lambda_i = H_i(T) - h_{c_i}(T) = -0.00020457T_i^2 - 2.473T_i + 2507 \quad (19)$$

$$h_{Li} = (4.187 - 2.26098X_i)T_{Li} \quad (20)$$

Using these above empirical correlations, the energy balance is defined as

For the first effect:

$$\frac{dT_1}{dt} = \frac{[\{L_2(4.187 - 2.26098X_2)(T_2 - T_1)\} + S\lambda_0(T_s) + V_1(4.15T_1 - H(T_1))]}{M_1(4.187 - 2.26098X_p)} \quad (21)$$

In a similar way, for second to sixth effects:

$$\frac{dT_i}{dt} = \frac{[\{L_{i+1}(4.187 - 2.26098X_{i+1})(T_{i+1} - T_i)\} + V_{i-1}\lambda_{i-1}(T_i) + V_i(4.15T_i - H(T_i))]}{M_i(4.187 - 2.26098X_i)}, \quad \text{Where i=2 to 6} \quad (22)$$

$$\text{Last effect: } \frac{dT_7}{dt} = \frac{[\{L_f(4.187 - 2.26098X_f)(T_f - T_7)\} + V_6\lambda_6(T_7) + V_7(4.15T_7 - H(T_7))]}{M_7(4.187 - 2.26098X_7)} \quad (23)$$

Hence, the developed model comprises a set of above determined nonlinear first order differential algebraic equations.

MODEL SOLUTION

The solution of the complex non-linear model described earlier is divided and explained below separately into solution of steady state and transient state.

1. Steady State Analysis

The solution of developed non-linear steady state MSE model, however, was quite challenging [45], and became even more complex especially, when the number of MSE stages increased leading to a higher number of equations to solve. GA is one kind of global optimization technique with the advantage of dealing with the integer variables; however, the interior-point method (I-PM) offers faster convergence rate and enables one to solve large-scale nonlinear program problems [46]. Therefore, we utilized the advantages of both the techniques (GA and I-PM) and evaluated the SE and SC with other steady state parameters (such as latent heat of vaporization, enthalpy and concentration per stage). The steady state parameters so computed and presented in this section enable the dynamic model development and solution, and help determine the transient response that is presented later in the next section.

1-1. Objectives and Constraints

To optimize the energy consumption of the MSE system, the objective function SE has been chosen, which needs to be maximized with optimum but feasible values of variables: vapor temperature, liquor flow rate and amount of fresh steam. In the previous literatures, an attempt was made to formulate the models and solve the single objective function (SC) optimization problem using genetic diversity evaluation method [47]. In this optimization problem, the focus was primarily to maximize the SE and minimize SC. The assumed cost function (SE) is hereby expressed by Eq. (24).

$$\text{Maximize } f_1(x) \Rightarrow \text{Minimize } \{-f_1(x)\} \quad (24)$$

f_1 returns the maximum of SE and minimum of SC to MSE system. Mathematically, SE is defined by Eq. (25).

$$f_1 = SE = \frac{\sum_{i=2}^{8} V_i}{V_1} \quad (25)$$

f_1 is a strong function of decision variables, x_i, which are: the amount of fresh steam supplied, V_1, and amount of vapor produced, V_i, $i \in \{2;7\}$. These vapor flow rates, V_i, $i \in \{2;7\}$ are functions of liquor flow rate, L_i, $i \in \{1;7\}$ and vapor temperatures at each effect, T_i, $i \in \{1;6\}$. Here, the decision variables, x_i, are assumed based on the maximum and minimum permissible bounds of feed liquor and fresh steam flow rates with their temperatures at each effect from available data. The inequality constraints, $g_i(x)>0$, are defined such that:

$$L_i < L_{i+1}, \ \forall \{i=1 \text{ to } 7\}, \ L_i > 0, \ \forall \{i=1 \text{ to } 7\} \quad (26)$$

Likewise, the equality constraints, $h_i(x)=0$, are based on the concept of setting the mass and energy balances to zero:

$$(L_i - L_{i-1})\lambda_i + L_{i+1}h_{i+1} - L_i h_i - (L_{i+1} - L_i)H_{i+1} = 0$$
$$U_i A_i(T_i - T_{i+1}) - (L_i - L_{i-1})\lambda_i = 0 \quad (27)$$

The selected feasible bounds based on available industrial data are: $T_i \in [100{:}110;\ 70{:}85;\ 66{:}74;\ 60{:}70;\ 55{:}65;\ 52{:}63] \forall \{i=2 \text{ to } 7\}$, and $L_i \in [2{:}5;\ 3.5{:}6;\ 4.5{:}7;\ 6.5{:}9;\ 9{:}11;\ 10.5{:}13;\ 13{:}15] \forall \{i=2 \text{ to } 7\}$. For the steam demand, the selected feasible bound is $V1 \hat{I} [0{:}3]$.

1-2. Interior Point Methodology (I-PM)

The objective function, $f_1(x)$ and constraints, x_i, should be continuously differentiable and satisfy Karush-Kuhn-Tucker (KKT)

conditions for the optimality of the problem [48,49]. The capability of I-PM was demonstrated earlier to solve the non-linear optimization problem with inequality and equality constraints [50-52]. In the present work, the formulated steady state model described in sub-section 1 of section Model Development was solved using the interior-point method (I-PM) after considering the optimization strategy and the steady state constraints mentioned in sub-section 1.1 of section Model Development. The data used for the simulation is tabulated in Table 1. In this method, a generalized form of the non-linear programming model [53] is given by Eq. (28).

$$\text{Subject to:} \quad \min_{x,\,s} f_1(X) \quad \begin{cases} C_E(x)=0 \\ C_I - S = 0 \\ \text{and, } s \geq 0 \end{cases} \tag{28}$$

The KKT conditions are defined by the Lagrangian function with constraints:

$$\begin{aligned} &\nabla f_1(x) - A_E^T(x)\lambda - A_I^T(x)z = 0 \\ &SZ - \mu e = 0 \\ &C_E(x) = 0 \\ &C_I - s = 0 \end{aligned} \tag{29}$$

Once the KKT condition is satisfied, then the sufficient condition should be met in which search direction (x, s, λ, z) is found using Newton's method as the barrier function to obtain the optimum problem solution.

$$\begin{bmatrix} W & 0 & -A_E^T(x) & -A_I^T(x) \\ 0 & Z & 0 & S \\ A_E(x) & 0 & 0 & 0 \\ A_I^T(x) & -I & 0 & 0 \end{bmatrix} \begin{bmatrix} d_x \\ d_s \\ d_\lambda \\ d_z \end{bmatrix} = \begin{bmatrix} \nabla f_1(x) - A_E^T(x)\lambda - A_I^T(x)z \\ SZ - \mu e \\ C_E(x) \\ C_I - s \end{bmatrix} \tag{30}$$

The value of (x, s, λ, z) is then updated after obtaining the previous values of (d_x, d_s, d_λ, d_z) and these updated values are utilized to evaluate optimality function by the norms.

$$d(x, s, \lambda, z, m) = \max\{\|\nabla f_1(x) - A_E^T(x)\lambda - A_I^T(x)z\| \times \|SZ - \mu e\| \times \|C_I - s\|\} \tag{31}$$

where, $\|\cdot\|$ represents the vector norm.

The I-PM algorithm has been described in detail and Schur-complement decomposition developed to address the optimization of high scale, nonlinear, block-structured problems with significant

Table 2. Steady state parameters of the BFF configured HEE models used for dynamic analysis

Steady state parameters	Methods used	Effect number						
		1	2	3	4	5	6	7
Liquor flow rate, L_i (in kg/sec)	I-PM	3.97	5.43	6.99	8.7	10.4	12.03	13.62
	GA	7.23	6.53	9.49	9.74	10.31	12.66	12.89
Temperature of vapor, T_i (°C)	I-PM	147	100.19	73.69	67.28	61.32	57.78	52
	GA	107.25	95.45	79.95	73.53	68.01	59.21	52
Latent heat of vaporization, λ_i (kJ/h)	I-PM	2109.51	2250.99	2323.5	2304.34	2355.62	2364.58	2372.97
	GA	2131.74	2230.75	2264.37	2306.93	2324.00	2338.44	2360.96
Vapor enthalpy, H_i (kJ/h)	I-PM	2678.67	2634.9	2623.8	2613.34	2607.03	2601.2	2596.63
	GA	2737.78	2684.50	2665.21	2639.77	2629.21	2620.11	2605.59
Liquor enthalpy, h_i (kJ/h)	I-PM	314.3	252.038	241.67	227.41	218.78	209.04	201.82
	GA	336.55	326.44	287.12	272.67	257.52	227.41	201.82
Concentration, X_i (% dry solids)	I-PM	0.46	0.34	0.26	0.21	0.18	0.15	0.13
	GA	0.30	0.33	0.23	0.22	0.21	0.17	0.16
SE	I-PM				**5.39**			
	GA				4.24			
SC (in kg/sec)	I-PM				2.16			
	GA				3			
Real plant data estimates (Star paper mill, Saharanpur, India)	SE				4.53-4.75[#]			
	SC (kg/sec)				2.67			
Previously reported simulated output	SE				5.56[a]			
	SC (kg/sec)				2.42[a]			

Note: The GA results has been used from published BFF model results [2]

[#]The SE has been reported in a range that considers the extreme values found between fouling and non-fouling (ideal) conditions

[a]Khanam and Mohanty Model [55]

number of mixed variables [54] (See Appendix A-1).

1-3. Solution Algorithm

To optimize the cost function, SE, a MATLAB programming code was developed which predicts the optimal values of T_i, L_i and V_1. The algorithm to compute SE was employed to compute these optimal values (See Appendix A-2). The obtained results through the simulation for SE, SC and other parameters using I-PM and GA are presented and compared with real-time plant data and previously reported simulation data in Table 2. Using these estimates, steady state parameters dynamic analysis was performed further.

2. Dynamic State Solution

2-1. State Space Representation

The system dynamics as determined from the described model are essentially nonlinear. Hence, before analyzing and simulating the system, the stability of the system must be analyzed. This requires determining the eigenvalues of the matrix **A** of the state space equation defined below:

$$\begin{aligned}\dot{x} &= Ax + Bu \text{ (state equation)}\\ y &= Cx + Du \text{ (output equation)}\end{aligned} \tag{32}$$

where the state, input and output vectors are derived from:

$$\left.\begin{aligned}x &= [x_1\ x_2\ x_3\ x_4\ x_5\ x_6\ x_7\ x_8\ x_9\ x_{10}\ x_{11}\ x_{12}\ x_{13}\ x_{14}]^T = \text{State variable}\\ u &= [L_f - L_{fs}\ X_f - X_{fs}\ T_f - T_{fs}\ S - S_s]^T = \text{Input variable}\\ y &= [y_1\ y_2\ y_3\ y_4\ y_5\ y_6\ y_7\ y_8\ y_9\ y_{10}\ y_{11}\ y_{12}\ y_{13}\ y_{14}]^T = \text{Output variable}\end{aligned}\right\} \tag{33}$$

$$\text{where, } x_m = \begin{cases} X_P - X_{Ps}, & m = 1\\ X_{j=2\text{ to }7} - X_{js=2\text{ to }7}, & 2 \le m \le 7\\ T_{j=1\text{ to }7} - T_{js=1\text{ to }7}, & 8 \le m \le 14\end{cases} \tag{34}$$

$$\text{and } y_m = \begin{cases} X_P - X_{Ps}, & m = 1\\ X_{j=2\text{ to }7} - X_{js=2\text{ to }7}, & 2 \le m \le 7\\ T_{j=1\text{ to }7} - T_{js=1\text{ to }7}, & 7 \le m \le 14\end{cases}$$

2-2. Stability and Controllability Analysis

The nonlinear dynamics of HEE system is represented through the Eq. (35).

$$\dot{x}_i = f_i(x_j, u_k),\ 1 \le i \le 14,\ 1 \le j \le 14 \text{ and } 1 \le k \le 4 \tag{35}$$

The eigenvalues of state space matrix **A** determined the stability of the system. The elements of matrix **A** are computed with the analytical linearization of the developed nonlinear dynamics using the partial differentiation of $f_i(x_j, u_k)$ with respect to state variable, x_j. Matrix **A** is a 14×14 matrix.

$$A_{ij} = \left.\frac{\partial f_i}{\partial x_j}\right|_{x_s},\ 1 \le i \le 14 \text{ and } 1 \le j \le 14 \tag{36}$$

A negative real part of the eigenvalue, ξ, contributes to a negative pole and ensures system stability. The value was evaluated and presented in Eq. (37), which clearly indicates a stable system under steady state:

$$\begin{aligned}\xi = [&-12.8025 + j4.7978 - 12.8025 - j4.7978 - 16.4128\\ &-17.2742 + j5.0789 - 17.2742 - j5.0789 - 21.6217\\ &+j8.7140 - 21.6217 - j8.7140 - 7.1460 - 9.7740 - 12.5820\\ &-15.6600 - 18.7200 - 21.6540 - 24.5160]^T\end{aligned} \tag{37}$$

Controllability of the HEE system means driving the dynamics from any arbitrary initial state to any desired final state in finite time. This has been evaluated using mathematical condition for controllability, called Kalman's controllability rank condition. In this condition, controllability matrix, $Q_c = [B : AB : A^2B : \ldots\ldots : A^{13}B]$, should assume its full rank. The present system described through its state-space representation of Eq. (32) was found to meet this criterion (rank $(Q_c) = 14$ and $|Q_c| = 0$), and hence, demonstrates controllability.

3. System Transfer Function Determination

The input-output transfer function in Laplace form is defined by:

$$G(s) = C(sI - A)^{-1}B \tag{38}$$

where the elements of matrix **B** correspond to the previously defined input variables, $u = [u_1\ u_2\ u_3\ u_4]^T$. It is analytically computed and found to be 14×4 matrix as represented by Eq. (39).

$$B_{ij} = \left.\frac{\partial f_i}{\partial u_j}\right|_{x_s},\ 1 \le i \le 14 \text{ and } 1 \le j \le 4 \tag{39}$$

The input-output transfer function, $g_{i1}(s)$, [i=1−7] relating the product concentration at various effects, X_p to X_7 to input feed flow rate, L_f, are computed and elaborated by Eqs. (40)-(46).

$$g_{11}(s) = \frac{-1194}{s^7 + 100.1s^6 + 5070s^5 + 1.266e05s^4 + 1.846e06s^3 + 1.57e07s^2 + 7.193e07s + 1.368e08} \tag{40}$$

$$g_{21}(s) = \frac{-122.2}{s^6 + 102.9s^5 + 4335s^4 + 9.56e04s^3 + 1.163e06s^2 + 7.388e06s + 1.914e07} \tag{41}$$

$$g_{31}(s) = \frac{-9.711}{s^5 + 93.13s^4 + 3425s^3 + 6.213e04s^2 + 5.556e05s + 1.958e06} \tag{42}$$

$$g_{41}(s) = \frac{-0.6201}{s^4 + 80.55s^3 + 2411s^2 + 3.179e04s + 1.55e05} \tag{43}$$

$$g_{51}(s) = \frac{-0.03313}{s^3 + 64.89s^2 + 1395s + 9938} \tag{44}$$

$$g_{61}(s) = \frac{-0.00153}{s^2 + 46.17s + 530.9} \tag{45}$$

$$g_{71}(s) = \frac{-6.24e\text{-}05}{s + 24.52} \tag{46}$$

It may be noticed that as we approach from last to first effect, the order of transfer function, increases from first- to seventh-order (1-7 poles) with no zeroes. However, the transfer function for the vapor temperature from T_1 to T_7 shows an increase from sixth- to thirteenth-order in numerator polynomial (6-13 zeroes) for a fourteenth-order in denominator polynomial (14 poles). This should reflect in a greater "lag" in dynamic vapor temperature than in the concentration. This draws a parallel with the physical observation that a change in liquor feed flow rate would first affect the product concentration before affecting the vapor temperature. In a similar fashion, the transfer functions relating the product concentration

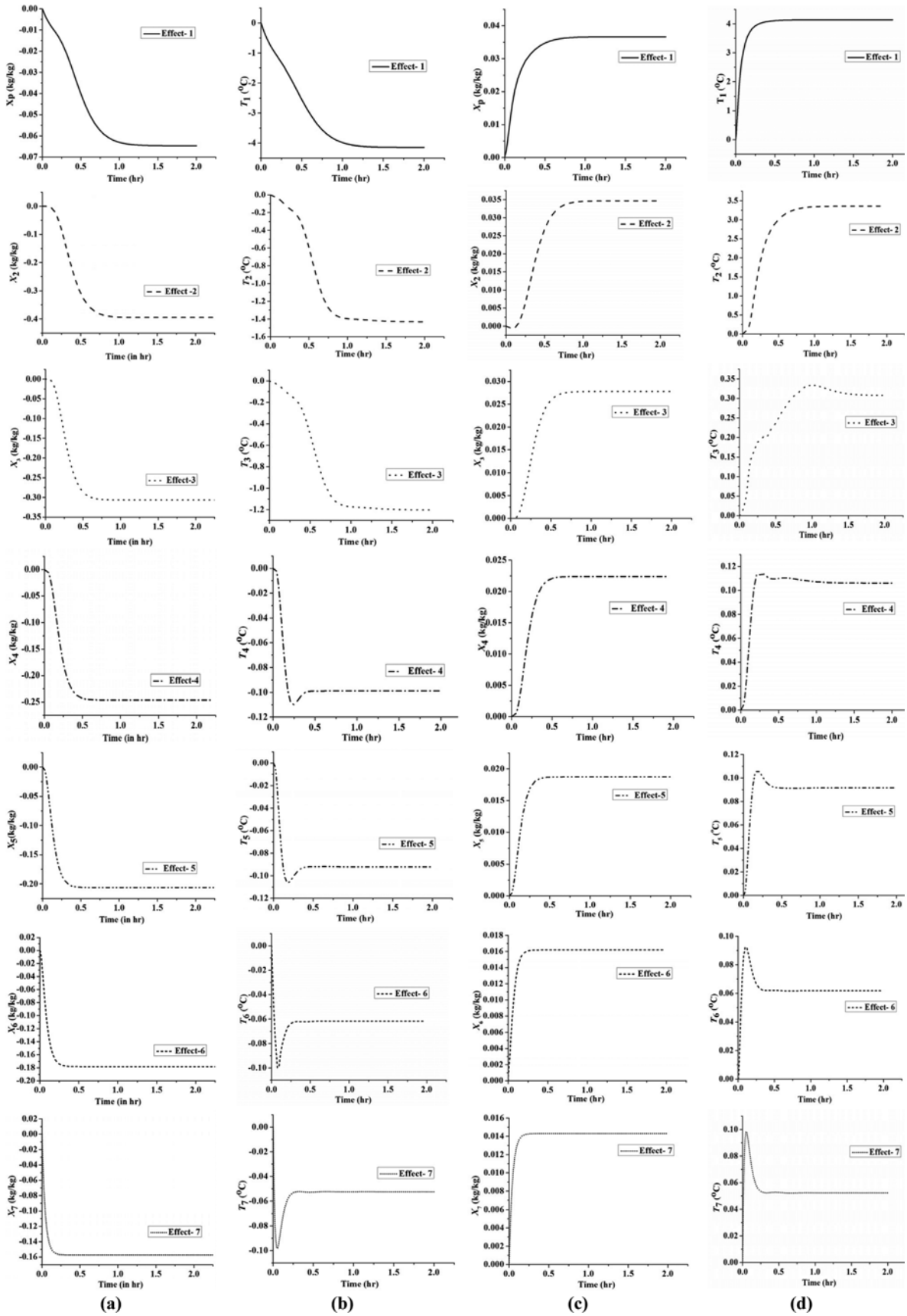

Fig. 2. Dynamic response (a) and (c) of deviations in product concentrations and (b) and (d) of deviations in generated vapor temperatures with a disturbance of ±10% in *liquor feed flow rate*.

and vapor temperature to other input variables have been determined but not presented here.

4. Control Strategy

To improve the system dynamics of variation in product concentration and vapor temperature for a change made in liquor feed flow, there is a need to implement a robust control strategy. A PID controller may be one good choice to speedily regulate the product concentration through feed liquor flow rate variation at the last stage based on the measured signal of product liquor concentration received by it [56,57]. The PID controller is one of the most commonly used industrial controllers and sends out a control signal, u(t), that depends on generated error, e(t). It consists of three parts: proportional, P, with output proportional to error, e(t), integral, I, with output proportional to weighted sum of all previous errors with integral time, T_i, and derivative term, D, proportional to derivative of error, with derivative time, T_d.

Mathematically, the compensated PID controller [58] in time and Laplace domain may be represented by Eqs. (47)-(48).

$$u(t) = K\left(e(t) + \frac{1}{T_i}\int_{i0}^{t} e(\tau)\,d\tau + T_d\frac{d}{dt}e(t) \right) \quad (47)$$

$$U = K\left(P + I\frac{1}{s} + D\frac{N}{1+N\frac{1}{s}} \right) \quad (48)$$

RESULTS AND DISCUSSION

The steady state system parameters obtained using I-PM were optimized at SE of 5.39 and SC of 2.16 kg/s as highlighted in Table 2. The presented steady state parameters serve as input initial condition to dynamic simulations attempted later. It is observed that I-PM shows better efficiency through improved SE (by ~24.8%) to solve such non-linear models compared to other optimization techniques, namely GA. This may be attributed to an improved search of parameter envelope for optimized conditions by I-PM.

The dynamic model was linearized, solved and its stability estimated around this steady state condition. To understand the dynamic performance and explore the response of product concentration and vapor temperature, a disturbance of ±10% was induced separately in liquor feed-flow rate, L_f, concentration, X_f, temperature, T_f and steam flow rate, S, from their steady state values of 56,200 kg/hr, 0.118% dry solid/total solid, 50 °C and 7,812 kg/hr respectively. The system dynamics during approach to a new steady state condition post the mentioned different disturbances was explored and described in following sub-sections.

1. Impact of Feed Flow Rate Variation

To understand the dynamic response of HEE, the influence of variation of liquor feed flow rate to last effect on the product concentrations, X_i (i=1-7) and vapor temperatures, T_i (i=1-7) at each effect were investigated. For this purpose, a variation of ±10% was made in the feed flow rate from 56,200 kg/hr and the dynamics of X_i's and T_i's for different effects simulated. Fig. 2(a) and 2(c) illustrate the effect observed for X_i's, while Fig. 2(b) and 2(d) represent the response of T_i's at different effects.

The simulations predict that product concentration, X_i (i=1-7) and vapor temperatures, T_i (i=1-7) increase for a decrease in feed flow rate and vice versa. The results also confirm that the dynamic of HEE system is open loop stable as also reflected by negative values of eigenvalues of matrix **A** estimated earlier. A comparison of time constant shown in Table 3 for the different effects reveals that the time constant for effects significantly increases as we move away

Table 3. Comparison of time constants, τ_i (i=1-7), of different effects for dynamic response of product concentrations, X_i (i=1-7) for a disturbance in feed rate, L_f

Parameters	Effect number						
	1	2	3	4	5	6	7
Time constant, τ_i, min (hr)	8.40 (0.14)	6.12 (0.102)	4.77 (0.0795)	3.84 (0.064)	3.18 (0.053)	2.76 (0.046)	2.46 (0.041)

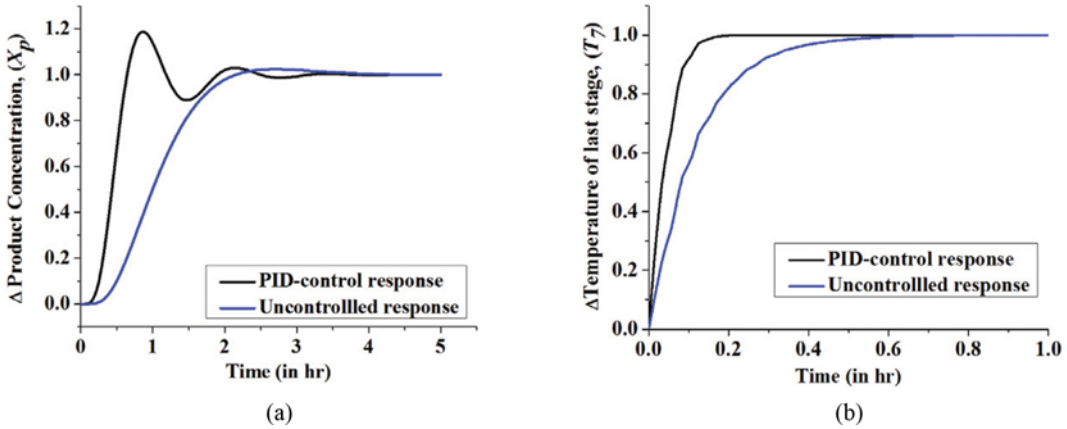

Fig. 3. Illustration of a PID control and uncontrolled system response of (a) product concentration and (b) last stage vapor temperature, for a set-point change made in liquor feed flow.

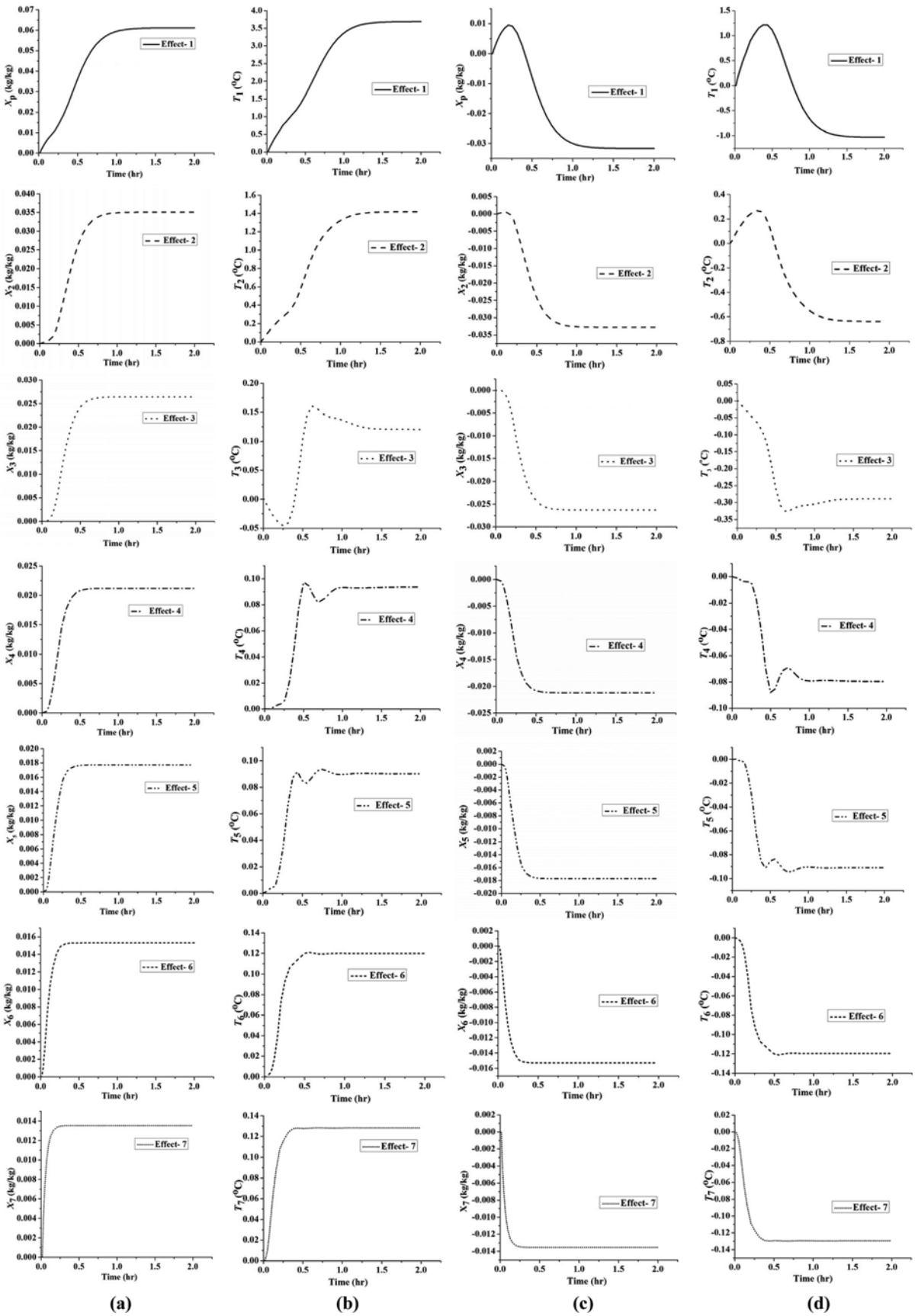

Fig. 4. Dynamic response (a) & (c) of deviations in product concentrations, X_i (i=1-7), and (b) & (d) of deviations in generated vapor temperatures, T_i (i=1-7), for a ±10% change in *liquor feed concentration*, X_f.

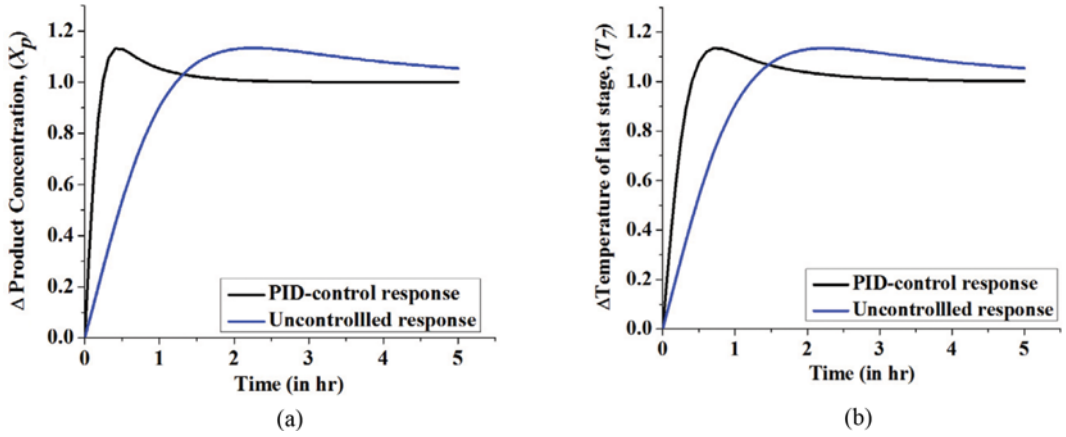

Fig. 5. Illustration of PID control and uncontrolled system response for variation in (a) product concentration and (b) last stage vapor temperature, for a set-point change made in liquor feed concentration.

from the source of disturbance (i.e., seventh effect) from τ_7=2.46 min to τ_1=8.40 min. This reveals the interactive nature of the system as is also evident from the nature of the curves.

The variation in concentration with simulation time is observed to be monotonically decreasing with increase in liquor flow rate and vice-versa. However, the vapor temperature with simulation time shows noticeable oscillations, while it decreases with increase in liquor flow rate and vice-versa. This interesting behavior prominently observed from the fourth-sevevnth effects may be attributed to the nonlinearity inherent in the system. Further, the nonlinearity increases while the effect number increases (from 1 to 7), as is also reflected in the increase in order (from 8-14) of system transfer functions.

A parallel form of PID controller was simulated which on tuning using Z-N method yields 1.12×10^5, 2.9×10^6 and 3.2×10^3 values for P, I and D actions. The value of coefficient, N, for parallel PID compensated filter in Laplace form was found to be 330.9 based on the overall transfer function already estimated. The controlled dynamic response was compared with the case when no control was employed for a set-point change in liquor feed flow. This is appropriately illustrated through Fig. 3. It is quite apparent that the controlled system response is much faster than the uncontrolled response in both the cases (variation in product concentration and last stage temperature). Although the control response for last stage vapor temperature does not show any undesirable overshoot, there is an apparent overshoot observed for PID-controlled response of product concentration. This implies that the product concentration, as against last stage vapor temperature, is relatively more sensitive to controller settings chosen.

2. Impact of Feed Concentration Variation

For the dynamic behavior of vapor temperatures, T_i (i=1-7), and product concentrations, X_i (i=1-7), at different effects, a disturbance of ±10% in the steady state feed concentration, X_f, (0.118 kg solids/kg of weak black liquor) is applied at the last effect. The results are presented in Fig. 4 wherein it is clearly seen that with constant supplied fresh steam and liquor flow rate, T_i and X_i (i=1-7) increase or decrease on increasing or decreasing X_f which is in line with the theoretical expectations.

To quantitatively compare the dynamic response at different effects, time constants, τ_i (i=1-7), were evaluated. The estimated values are presented in Table 3 and are to be found similar to the values determined as in sub-section 1 of Results and Discussion section. The estimates reveal that time constant for effects significantly increases as we move away from the source of disturbance (i.e., seventh effect) from τ_7=2.46 min to τ_1= 8.40 min. This reveals the interactive nature of the system, as is also evident from the nature of curves. Further, the similar values of τ_i (i=1-7), for dynamic response of T_i's and X_i's, for disturbance in X_f and L_f, are attributed to the fact that both correspond to making a change in the water or solids component flow rate that translates into a similar change in evaporation rates and finally into changes in vapor temperatures, T_i's.

The simulated time domain transient responses of the MSE to control the product concentration and vapor temperature using PID controller considering with liquor feed concentration are shown in Fig. 5. The specifications used to design the PID controller are following: $P=1.38\times10^5$, $I=2.1\times10^5$, $D=-3.6\times10^4$ and filter coefficient, N=13.44. Fig. 5 compares the PID controller dynamic response with the case when no control is employed for a set-point change in feed concentration. The controlled response is evidently much faster than the uncontrolled response for both the cases of variation in product concentration and last stage vapor temperature.

3. Impact of Feed Temperature Variation

To understand the dynamic behavior of vapor temperature of effects, T_i (i=1-7), a ±10% variation in the black liquor feed temperature, T_f, was made. The impact on T_i's due to T_f variation is illustrated in Figs. 6 and 7, wherein it is understood that vapor temperatures in different effects do not undergo a noticeable variation.

The trend presented indicates that vapor temperatures increase (Fig. 6) or decrease (Fig. 7) with an increase or decrease in liquor feed temperature. Since, in our model, the feed temperature is not mathematically related to product concentrations in any of the effects, hence, no variation was observed in product concentrations. This observation draws parallel with similar previous results [10].

4. Impact of Fresh Steam Flow Rate Variation

To study the dynamic behavior of generated vapor temperatures, T_i (i=1-7), a +10% disturbance in fresh steam steady state flow rate,

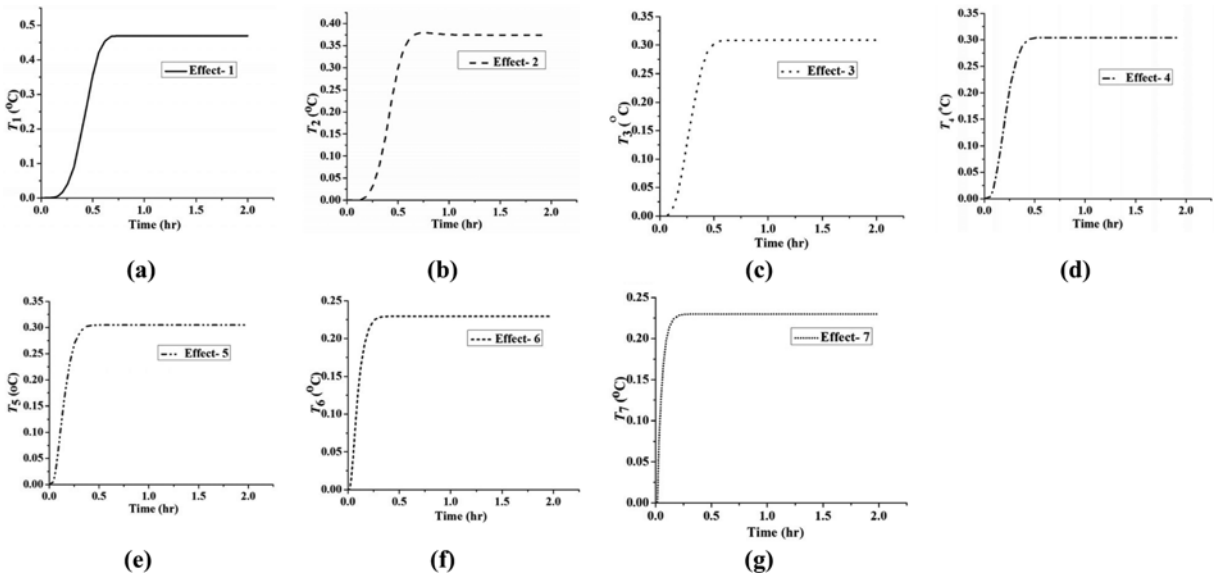

Fig. 6. Dynamic response of deviations in temperatures of generated vapors, T_i (i=1-7), for a +10% change in *liquor feed temperature*, T_f.

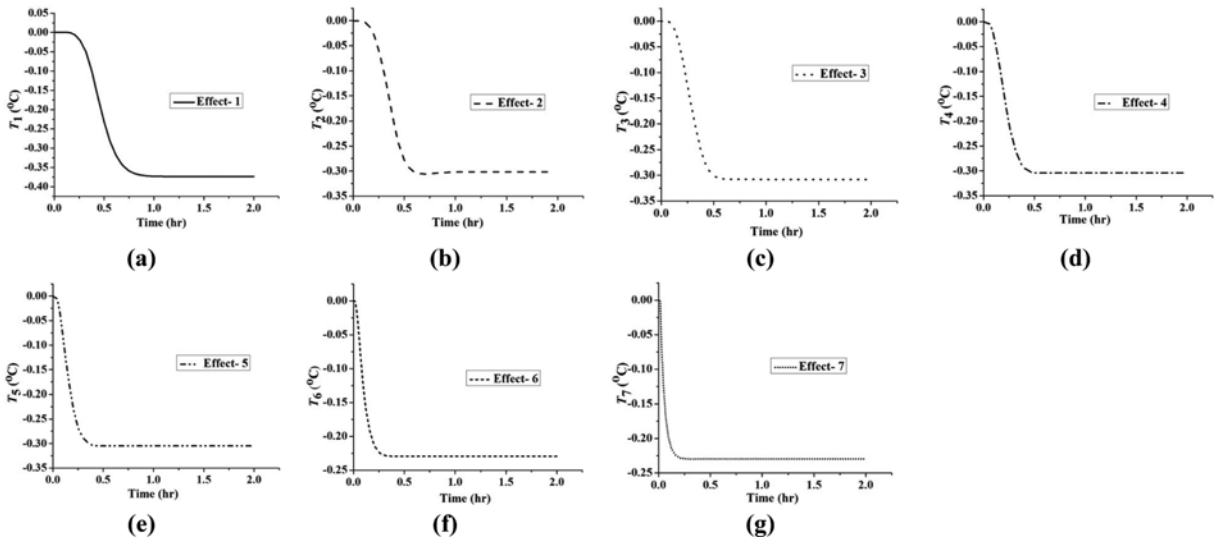

Fig. 7. Dynamic response of deviations in temperatures of generated vapors, T_i (i=1-7), for a −10% change in *liquor feed temperature*, T_f.

S (7,812 kg/hr) was made. The dynamic response is presented in Fig. 8, which is similar to the response observed for a variation of the fresh feed flow rate, L_f, although reversed in direction due to change of disturbance source.

The response is seen to get faster as we move from first effect to last, the first effect displaying a clear first order response and the later effects showing interactive higher order responses. The effect of steam flow rate on the vapor temperatures, T_i (i=1-7), was found to vary from ~35-2.5 °C in first to last effects. The deviations in T_i's show a decrease from first effect (T_1=35 °C) to last effect (T_7=2.7 °C), which may be attributed to the decrease in steady state T_i values for each effect.

The controlled dynamic response was compared with the case when no control is employed for a change in liquor feed flow. This is appropriately illustrated through Fig. 9, wherein it is quite evident that the controlled system response is much faster than the uncontrolled response for last stage temperature, as illustrated through a shorter rise time and response time of the former than the latter. However, the controlled response shows a marginal overshoot that settles reasonably quickly. A control of last stage temperature inherently implies control of concentration of product derived at the last stage.

SUMMARY AND CONCLUSIONS

The present work attempts to develop the dynamics of backward feed flow HEE for pulp and paper mills. The first principle of thermodynamics translates the model into a set of fourteen nonlinear first-order differential algebraic equations. The steady state analysis indicates that the search technique (I-PM versus GA, etc.) could

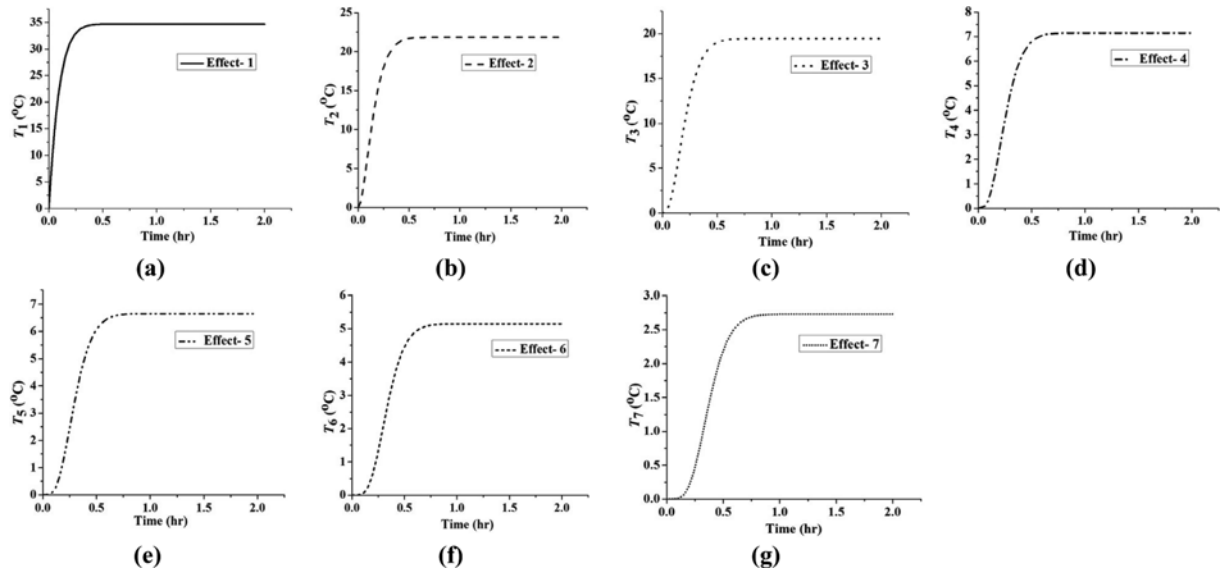

Fig. 8. Dynamic response of deviations in vapor temperatures, T_i, for a +10% change in *fresh steam flow rate*, S.

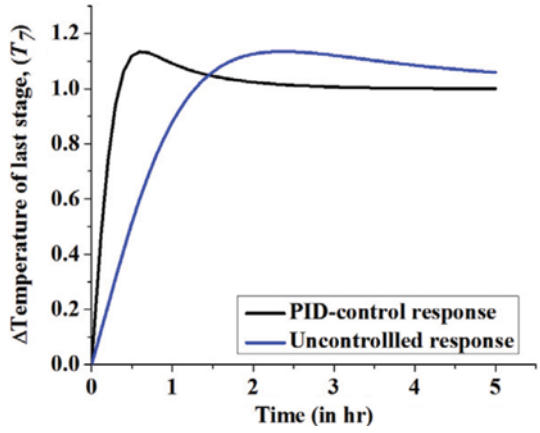

Fig. 9. Illustration of a PID control and uncontrolled system response for variation in last stage vapor temperature, for a set-point change made in liquor feed flow.

influence strongly the determination of optimized process conditions, and hence, ensuring energy savings for MSE. The state space technique has been then employed to analyze the developed dynamic model. The eigenvalues of the state space matrix show that the system is regulated around the steady state point, and the system controllability is established.

The impact of process disturbances--flow rate, concentration and temperature of black liquor feed and fresh steam flow rate--was then studied on the product concentrations, X_i (i=1-7) and vapor temperatures, T_i (i=1-7). The X_i's and T_i's were found to vary between 1.2-6% and 1.2-4%, respectively, on disturbing feed flow rate by ±10%. Also, the dynamic response was interactive and progressively became slower from last to first effects. Further, a disturbance of ±10% in feed concentration, X_f made the X_i's and T_i's deviate from their steady state values from 1.3-6% and 1.2-4%, respectively. However, disturbing the steam flow rate with a ±10% change induced relatively very high deviations (5.2-34.5%) in T_i's that may be attributed to the higher enthalpy flow rate associated with the input steam rather than the input liquor feed. Hence, it may be concluded that the steam flow rate is the major controlling factor that governs product concentration and effect temperatures, and so needs accurate and careful control to maintain process conditions and product quality. Further, the simulations of the dynamic model provide us an idea of process parameters across various effects such as order of time constants (or delay) during which the disturbances will traverse the effects. This practically helped to identify liquor flow rate as the controller tuning or manipulating parameter. An implementation of PID control strategy was found to significantly improve the system dynamic response.

ACKNOWLEDGEMENTS

Mr. Om Prakash Verma would like to thank the Ministry of Human Resource Development, New Delhi, India for providing the Senior Research Fellowship for this work and Graphic Era University, Dehradun to grant study leave to pursue Ph.D. Also, the authors are thankful to the Director of Star Paper Mill, Saharanpur, India for permissions to visit the mill time to time and collect the real-time plant data. The authors would like to acknowledge Prof. A. K. Ray (Department of Polymer and Process Engineering) from Indian Institute of Technology Roorkee for some of his useful suggestions and discussions related to the problem.

NOMENCLATURE

A : heat transfer area [m^2]
A : state matrix
B : input matrix
A_E (**x**): jacobian matrix of C_E (**x**)
A_I (**x**) : jacobian matrix of C_I (**x**)
C : output matrix
C_E (**x**): A set of equality constraints

C_I (**x**) : A set of inequality constraints
d : descent direction
D : feedthrough matrix
e : Error (a size of n vector, $[1\ 1\ 1 \ldots\ldots 1]^T$)
f : function
g : transfer function
GJ : giga joule
GWh : giga watt hour
h : enthalpy [kJ/kg]
H : enthalpy of vapor [kJ/kg]
kWh : kilo watt hour
L : feed flow rate [kg/hr]
Mtpa : mega ton per annum
Q_c : controllability matrix
s : laplace operator
s : a vector of nonnegative slack variables
S : diagonal matrix of order n×n containing a vector of non-negative slack variable
S : fresh steam flow rate [kg/hr]
SC : steam consumption [kg/hr]
SE : steam economy
T : vapor body temperature [°C]
u : input variables
U : overall heat transfer coefficient [kW/ m^2 °C]
V : vapor flow [kg/hr]
W : hessian matrix
x : state variable
x : decision variables
X : concentration [% dry solid in kg/total solid in kg]
Y : output variable
z : vector of Lagrangian multiplier for C_I
Z : diagonal matrix contains vector z

Subscripts

i : effect number
j : imaginary unit
f : feed
s : steam
p : product
L : liquor
c : condensate

Greek Letters

λ : latent heat of vaporization [kJ/kg]
$\boldsymbol{\lambda}$: vector of Lagrangian multiplier for C_E
Δ : change/difference
ξ : eigen value
μ : the barrier parameter
∇ : divergence
τ : time constant

REFERENCES

1. T. Johnson, B. Johnson and K. H. A. Mukherjee, India - An emerging giant in the pulp and paper industry. 65th Appita Annu Conf Exhib Rotorua New Zeal 10-13 April 2011 Conf Tech Pap 2011:135. http://webcache.googleusercontent.com/search?q=cache:4wppefVmJTkJ:becaamec.co.nz/media/~/media/beca_amec/media/technical_papers/india_emerging_giant_pulp_paper_industry.ashx+&cd=5&hl=en&ct=clnk&gl=in.
2. O. P. Verma, Suryakant, G. Manik, *Int. J. Syst. Assur. Eng. Manage.*, 1 (2016), DOI:10.1007/s13198-016-0533-0.
3. J. Laurijssen, A. Faaij and E. Worrell, *Appl. Energy*, **98**, 102 (2012).
4. G. Jyoti and S. Khanam, *Int. J. Therm. Sci.*, **76**, 110 (2014).
5. P. Sarkar, S. Datta, C. Bhattacharjee, P. K. Bhattacharya and B. B. Gupta, *Korean J. Chem. Eng.*, **23**, 617 (2006).
6. M. Naqvi and E. Dahlquist, *Appl. Energy*, **90**, 24 (2012).
7. D. J. Marshman, T. Chmelyk, M. S. Sidhu, R. B. Gopaluni and G. A. Dumont, *Appl. Energy*, **87**, 3514 (2010).
8. J. W. Kim, S. B. Lalvani and B. A. Akash, *Korean J. Chem. Eng.*, **12**, 582 (1995).
9. I. J. Esfahani, J. Rashidi, P. Ifaei and C. Yoo, *Korean J. Chem. Eng.*, **33**, 351 (2016).
10. D. Kumar, V. Kumar and V. P. Singh, *Appl. Math. Model*, **37**, 384 (2013).
11. H. T. El-Dessouky and H. M. Ettouney, *Desalination*, **125**, 259 (1999).
12. Y.-C. Huang, C.-I. Hung and C.-K. Chen, *Proc. Inst. Mech. Eng. Part A J. Power Energy*, **214**, 61 (2000).
13. R. Sharma and S. Mitra, *Int. J. Green Energy*, **2**, 109 (2005).
14. R. Bhargava, S. Khanam, B. Mohanty and A. K. Ray, *Comput. Chem. Eng.*, **32**, 2203 (2008).
15. X. Ding, W. Cai, L. Jia and C. Wen, *Appl. Energy*, **86**, 81 (2009).
16. S. Khanam and B. Mohanty, *Desalination*, **262**, 64 (2010).
17. S.-Y. Wu, L. Jiang, L. Xiao, Y.-R. Li and J.-L. Xu, *Int. J. Green Energy*, **9**, 780 (2012).
18. D. Srivastava, B. Mohanty and R. Bhargava, *Chem. Eng. Commun.*, **200**, 1089 (2013).
19. D. Xevgenos, P. Michailidis, K. Dimopoulos, M. Krokida and M. Loizidou, *Desalin Water Treat*, **53**, 3407 (2015).
20. O. P. Verma, T. H. Mohammed, S. Mangal and G. Manik, *Int. J. Syst. Assur. Eng. Manage.*, 1 (2016).
21. J. Oh, I. S. Ye, S. Park, C. Ryu and S. K. Park, *Korean J. Chem. Eng.*, **31**, 2136 (2014).
22. D. Kaya and H. Ibrahim Sarac, *Energy*, **32**, 1536 (2007).
23. S. Khanam and B. Mohanty, *Appl. Energy*, **87**, 1102 (2010).
24. M. Karlsson, *Appl. Energy*, **88**, 577 (2011).
25. R. N. Lambert, D. D. Joye and F. W. Koko, *Ind. Eng. Chem. Res.*, **26**, 100 (1987).
26. G. Gautami and S. Khanam, *Desalination*, **288**, 16 (2012).
27. W. O. Ayangbile, E. O. Okeke and G. S. G. Beveridge, Pergamon, 8 (1984), DOI:10.1016/0098-1354(84)87011-8.
28. M. Higa, A. J. Freitas, A. C. Bannwart and R. J. Zemp, *Appl. Therm. Eng.*, **29**, 515 (2009).
29. C.-I. Tuan, Y.-L. Yeh, L.-F. Hsu and T.-C. Chen, *Korean J. Chem. Eng.*, **29**, 341 (2012).
30. J. A. Winchester and C. Marsh, *Dyn. Control*, 77 (1999), DOI:10.1205/026387699526340.
31. H. Andre and R. A. Ritter, *Can. J. Chem. Eng.*, **46**, 259 (1968), DOI:10.1002/cjce.5450460409.
32. H. Shin, Y. K. Lim, S.-K. Oh, S. G. Lee and J. M. Lee, *Korean J. Chem. Eng.*, **34**, 287 (2017).

33. R. B. Newelll and D. G. Fisher, *Ind. Eng. Chem. Process Des. Dev.*, **11**(2), 213 (1972).
34. Y. Izawa and K. Hakomori, *Trans. Soc. Instrum Control Eng.*, **32**, 197 (1996).
35. L. C. To, M. O. Tadé and G. P. Le Page, *Control Eng. Pract*, **6**, 1309 (1998).
36. G. J. Adams, B. J. Burke and G. C. Goodwin, *The International Federation of Automatic Control*, **41** (2008), DOI:10.3182/20080706-5-KR-1001.02356.
37. O. P. Verma, T. M. Haji, S. Mangal and G. Manik, *Int. J. Control Theory Appl.*, **9**, 5287 (2016).
38. P. Yadav and A. K. Jana, Chemical Product and Process Modeling Simulation and Control of a Commercial Double Effect Evaporator: Tomato Juice, 5 (2010), DOI:10.2202/1934-2659.1443.
39. Z. Stefanov and K. A. Hoo, *Ind. Eng. Chem. Res.*, **44**, 3146 (2005).
40. N. Russell, H. Bakker and R. Chaplin, *Chem. Eng. Res. Des.*, **78**, 1120 (2000).
41. A. O. S. Costa and E. L. Lima, *Can. J. Chem. Eng.*, **81**, 1032 (2008).
42. C. H. Runyon, T. R. Rumsey and K. L. McCarthy, *J. Food Eng.*, **14**, 185 (1991).
43. V. Miranda and R. Simpson, *J. Food Eng.*, **66**, 203 (2005).
44. O. P. Verma, T. H. Mohammed, S. Mangal and G. Manik, Mathematical Modeling of Multistage Evaporator System in Kraft Recovery Process. In: Proc. Fifth Int. Conf. Soft Comput. Probl. Solving SocProS 2015, Vol. 2, Singapore: Springer Singapore; 2016, p. 1011-42.
45. A. Pourrajabian, R. Ebrahimi, M. Mirzaei and M. Shams, *Appl. Math. Comput.*, **219**, 11483 (2013), DOI:10.1016/j.amc.2013.05.057.
46. W. Yan, F. Liu, C. Y. Chung and K. P. Wong, *IEEE Trans Power Syst.*, **21**, 1163 (2006).
47. S. Mesfun and A. Toffolo, *Appl. Energy*, **107**, 98 (2013).
48. H. W. Kuhn and A. Tuckerm *Proc. Second Symp. Math. Stat. Probab.*, 481 (1951), DOI:10.1007/BF01582292.
49. O. P. Verma, T. H. Mohammed, S. Mangal and G. Manik, *Energy*, **129**, 148 (2017).
50. J. S. Albuquerque, V. Gopal, G. H. Staus, L. T. Biegler and B. Erik Ydstie, *Comput. Chem. Eng.*, **21**, S853 (1997).
51. M. Kojima, N. Megiddo and S. Mizuno, *Math Program*, **61**, 263 (1993).
52. A. Kusiak, G. Xu and Z. Zhang, *Energy Convers. Manage.*, **85**, 146 (2014).
53. I. E. Grossmann, J. A. Caballero and H. Yeomans, *Korean J. Chem. Eng.*, **16**, 407 (1999).
54. J. Kang, Y. Cao, D. P. Word and C. D. Laird, *Comput. Chem. Eng.*, **71**, 563 (2014).
55. S. Khanam and B. Mohanty, *Comput. Chem. Eng.*, **35**, 1983 (2011).
56. O. P. Verma, G. Manik and V. K. Jain, *J. Comput. Sci.*, (2017), DOI:10.1016/j.jocs.2017.04.001.
57. O. P. Verma, T. H. Mohammed, S. Mangal and G. Manik, *Trans. Inst. Meas Control*, 142331217700239 (2017), DOI:10.1177/0142331217700239.
58. O. P. Verma, S. Kumar and G. Manik, Analysis of Hybrid Temperature Control for Nonlinear Continuous Stirred Tank Reactor. Proc. Fourth Int. Conf. Soft Comput. Probl. Solving SocProS 2014, Vol. 2, New Delhi: Springer India, 103 (2015).

APPENDIX

***Appendix A-1: Algorithm* for Executing Interior Point Method**

1. **Start** with the initial points of $(x^0, s^0, \lambda^0, z^0)$ with $x^0, s^0, \lambda^0, z^0>0$

Set the initial value of barrier parameter and tolerance constant $\mu_0>0$ and ε_{tol}, $n\varepsilon>0$

Assuming the maximum number of iterations is n_{max}

2. **Set** the iteration $n\leftarrow 0$

3. **Condition** for the convergence of optimization problem:

if $E(x^n, s^n, \lambda^n, z^n; \mu_n)<\varepsilon_{tol}$, *then*, optimum solution exist

Condition for the convergence of barrier function:

if $E(x^n, s^n, \lambda^n, z^n; \mu_n)<n_\varepsilon\mu^n$, *then*, only update μ^n using Eq. (31) and return to verify the convergence condition of optimization problem

4. **Compute**: $f_1(x^n)$, $C_E(x^n)$, $C_I(x^n)$, $A_E^T(x^n)$, $\nabla f_1(x^n)$ and $\nabla^2_{xx}\mathcal{L}(x^n, \lambda^n)$

Evaluate the search direction 'd': $(d_x, d_s, d_\lambda, d_z)$ using Eq. (31) and update the step size value and continue for the maximum iterations n+1

5. **Evaluate**: $(x^{n+1}, s^{n+1}, \lambda^{n+1}, z^{n+1})$ and also, $\mu^{n+1}\leftarrow\mu^n$ and $n+1\leftarrow n$

If $n<n_{max}$, then exit otherwise,

Return to **Condition** for the convergence of barrier function (Step 3)

***Appendix A-2:* Estimation of Steam Economy (SE)**

1. **Require**: Area of each effect

2. **Initialize** with equal ΔT_i, L_i, x_i at each effect

3. **Guess** the value of U using available correlation,

$$U=2000\left(a\left(\frac{\Delta T}{40}\right)^b\left(\frac{x_{avg}}{0.6}\right)^c\left(\frac{L_{avg}}{25}\right)^d\right)$$

4. **while** $\left(\frac{U_{new}-U_{old}}{U_{old}}\right)100>0.1$ // stopping criteria

for each effect do

$\lambda_i=-0.003857T_i^2-2.069T_i+2497$

$H_i=-0.0002045T_i^2+1.677T_i+2507$

$h_{Li}=4.187\ (1-0.54x_i)T_i$

end for

Compute: Maximize $f_1(x)\Rightarrow$Minimize$\{-f_1(x)\}$, // using Interior point method algorithm

$$f_1=SE=\frac{\sum_{i=2}^{8}V_i}{V_1}$$

Subject to:

Equality constraints: Based on mass and energy balances equated to zero with different operating strategies

Inequality constraints: $T_i>T_{i+1}$, $\forall\{i=1, 2, \ldots 5\}$ and $T_6>52$ (T_7), $T_i>0$, $\forall\{i=1, 2, \ldots 6\}$, $L_i<L_{i+1}$, $\forall\{i=1, 2, \ldots 7\}$, $L_i>0$, $\forall\{i=1, 2, \ldots 7\}$.

5. **Evaluate**: $T_i\leftarrow T_i$, $L_i\leftarrow L_i$ and $x_i\leftarrow x_i$

6. **Evaluate**: new $U\leftarrow 2000\left(a\left(\frac{\Delta T}{40}\right)^b\left(\frac{x_{avg}}{0.6}\right)^c\left(\frac{L_{avg}}{25}\right)^d\right)$ using new T_i, L_i and x_i

end while

return SE, T_i, L_i and x_i